

Nikhef 2013-037

# An extended Heitler-Matthews model for the full hadronic cascade in cosmic air showers.

J.M.C. Montanus

Nikhef

November 4, 2013

## Abstract

The Heitler-Matthews model for hadronic air showers will be extended to all the generations of electromagnetic subshowers in the hadronic cascade. The relation between interaction length and the thickness of the cascade layers is revisited. The analysis is outlined in detail for showers initiated by primary protons. For showers initiated by iron primaries the part of the analysis is given for as far as it differs from the analysis for a primary proton. Predictions for shower sizes and the depth of maximum shower size are compared with results Monte Carlo simulations. As for the Heitler-Matthews model the present model predicts too small values for the depth of maximum shower size. The application of the Heitler-Matthews model to the first generation of electromagnetic subshowers leads to an overestimation of the elongation rate. The application of the Heitler-Matthews model to all the generations of electromagnetic subshowers results in an elongation rate which decreases for increasing energy. The discrepancy with respect to predictions from Monte Carlo models can therefore not be explained from the neglectance of the second and higher generations in the hadronic cascade. An alternative explanation will be proposed.

# 1 Introduction

A simplified description of the longitudinal evolution of electromagnetic showers is given by the Heitler model [1]. Starting with a primary particle of energy  $E_0$ , the number of particles doubles every splitting length  $d = \lambda_r \ln 2$ , where the radiation length  $\lambda_r$  is about  $37 \text{ g cm}^{-2}$ . The doubling stops when the energy per particle is equal to the critical energy  $\xi_c^e \approx 85 \text{ MeV}$ . The resulting Heitler profile is

$$N(X) = \begin{cases} 2^{X/d} & , X \leq n_c^e d ; \\ 0 & , X > n_c^e d , \end{cases} \quad (1)$$

where  $n_c^e$  is maximum the number of steps:  $n_c^e \ln 2 = \ln(E_0/\xi_c^e)$ .

A Heitler model for the hadronic cascade in air showers has been constructed by Matthews [2]. The Heitler-Matthews model is useful for the explanation of hadronic cascades as well as for the analytical derivation of relations between quantities as primary energy, muon number, electron number and depth of maximum shower size [3, 4, 5]. For the prediction of the number of charged particles it is assumed that each hadronic interaction results in  $M_{\text{ch}} = 10$  charged pions and  $\frac{1}{2}M_{\text{ch}} = 5$  neutral pions. That is, the total multiplicity  $M$  is equal to 15. The neutral pions initiate electromagnetic subshowers when they decay into photons. For the prediction for the depth of maximum shower size, restricted to the first generation of electromagnetic subshowers, the multiplicity and interaction length are parameterized by the energy of the interaction.

The atmosphere is divided into layers of atmospheric thickness  $d_I$ . After the traversing of each layer the number of charged pions are assumed to be  $M_{\text{ch}}$  times larger if  $d_I = \lambda_I \ln 2$ , where  $\lambda_I = 120 \text{ g cm}^{-2}$  is the interaction length of strongly interacting pions. Consequently, after  $n$  layers the number of charged pions is  $(M_{\text{ch}})^n$ . The energy per pion is

$$E_{\pi,n} = \frac{E_0}{M^n} . \quad (2)$$

The stopping energy is estimated on the basis of the finite lifetime of the pions in the atmosphere. For this it suffices to consider the approximate relation between atmospheric depth and height:

$$X(h) = 1030 \cdot e^{-h/8} \leftrightarrow h(X) = 8 \ln(1030/X) , \quad (3)$$

where  $X$  is the depth in  $\text{g cm}^{-2}$  and  $h$  is the height in km. Neutral pions decay almost immediately into two photons,  $c\tau = 25 \text{ nm}$  [6]. Each resulting photon starts an electromagnetic shower. The decay length of the charged pions is  $c\tau = 7.8 \text{ m}$  [6]. The actual length is substantially larger because of

the relativistic time dilation. As a consequence charged pions may interact with the atmosphere and propagate the hadronic shower, before decay. If the probability for decay in the next layer is larger than the probability of a hadronic interaction, the pions are assumed to decay and the cascade stops. This happens after  $n_c$  layers. The corresponding energy of the decaying charged pions, the stopping energy  $\xi_c^\pi$ , follows from

$$\xi_c^\pi = \frac{E_0}{M^{n_c}} . \quad (4)$$

The stopping energy turns out to be around 20 GeV.

## 2 Model parameters

In this paper the Heitler-Matthews model is extended to all the generations of pions in the shower. The complete analysis will be based on the situation where the multiplicity  $M$  and interaction length  $\lambda_I$  depend on the energy of the hadron in the shower. One of the consequences is that the thickness of the cascade layers increases with depth, see Fig. 1.

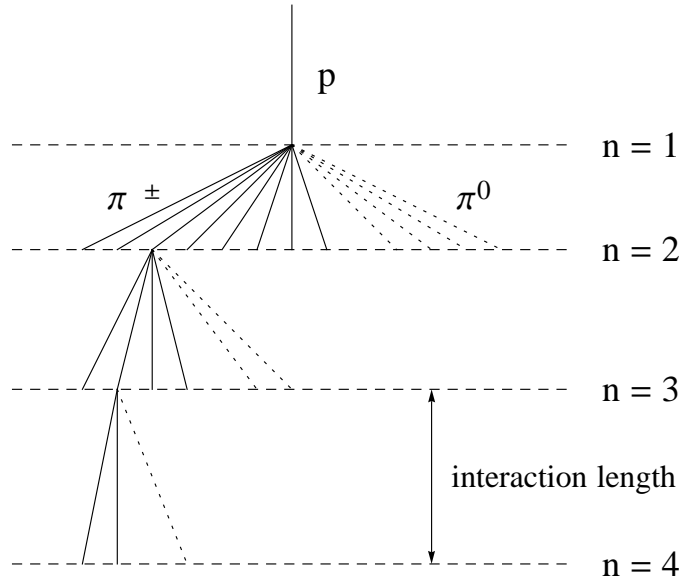


Figure 1: The hadronic cascade for energy dependent interaction lengths.

For the present model we will consider the energy dependence of the  $\pi$ -air multiplicity and interaction length as calculated by Monte Carlo event generators based on QCD and parton models. The calculated  $\pi$ -air charged multiplicity, see Fig. 5 of [7], Fig. 7 of [8] and Fig. 5 of [9], suggests the

relation

$$M_{\text{ch}} \approx 0.1 \cdot E^{0.18} , \quad (5)$$

where  $E$  is the energy in eV. Taking the ratio of the charged and neutral pions as 2 : 1, we have for the total multiplicity

$$M \approx 0.15 \cdot E^{0.18} , \quad (6)$$

It should be emphasized that the relation between multiplicity and energy is rather uncertain since different models predict different multiplicities. In particular for large energies the differences can be large, even more than 100%. From Fig. 5 of [7] and Fig. 7 of [8] we see that the pion multiplicity does not differ substantially from the proton multiplicity. We therefore will use the relations (5) and (6) for both the multiplicity in proton-air (p-air) and pion-air ( $\pi$ -air) interactions. A parameterization with other values for the constants will, of course, affect the results quantitatively. It does, however, not alter the results qualitatively.

Both the p-air and  $\pi$ -air production cross sections grow with energy. The p-air production cross section at large energies obtained from observations of extensive air showers are in good agreement with QGSJET predictions [10, 11, 12, 13]. For the present analysis we will therefore use the QGSJET predictions for the p-air production cross section. We will also use the QGSJET predictions for the  $\pi$ -air production cross section [8, 14]. From these cross sections approximations for the interaction lengths can be derived which are sufficiently accurate for our purpose. For  $\pi$ -air this is:

$$\lambda_{\pi\text{-air}} [\text{g cm}^{-2}] \approx 200 - 3.3 \ln(E[\text{eV}]) . \quad (7)$$

For p-air this is

$$\lambda_{\text{p-air}} [\text{g cm}^{-2}] \approx 145 - 2.3 \ln(E[\text{eV}]) . \quad (8)$$

In these equations the energy  $E$  is in eV. A practical reason for writing the multiplicity as a power of the energy  $E$  and the interaction length linear in  $\ln E$  is the convenience for the present analysis. Before we turn to the analysis we first consider general multiplicative growth processes for fixed interaction lengths and several fixed multiplicities.

### 3 Multiplication statistics

In this section we will revisit the relation  $d_I = \lambda_I \ln 2$  as it is used in the Heitler-Matthews model for hadronic air showers [2, 3]. The latter might be motivated by the expression  $\lambda_r \ln 2$  for the splitting length in the electromagnetic cascade. There the ratio  $\ln 2$  results from the translation of

the radiation length to the splitting length. In an intermediate model for electromagnetic showers the splitting length,  $\lambda_r \ln 2$ , is effectively used as the electromagnetic interaction length [15]. For the hadronic cascade, however, there is no a priori reason for the ratio  $\ln 2$  between layer thickness and interaction length. Since  $\lambda_I$  is already an interaction length, the ratio between layer thickness and interaction length is rather expected to be 1. For certainty we investigate the ratio by means of a pure mathematical multiplication model.

Assuming interactions occur randomly with an average atmospheric depth interval  $\lambda_I$ , the number of interactions in a layer of the atmosphere with a thickness  $X$  is Poisson distributed with the interaction length  $\lambda_I$  as the parameter:

$$P(k) = \frac{1}{k!} \left( \frac{X}{\lambda_I} \right)^k e^{-\frac{X}{\lambda_I}} . \quad (9)$$

If each interaction produces  $M_{\text{ch}}$  charged particles and if the number of interactions is unlimited, the expectation value of the number of charged particles at depth  $X$  would be

$$N = \sum_{k=0}^{\infty} \frac{1}{k!} \left( \frac{M_{\text{ch}} X}{\lambda_I} \right)^k e^{-\frac{X}{\lambda_I}} \equiv e^{\frac{X}{\lambda_I} (M_{\text{ch}} - 1)} . \quad (10)$$

Obviously, without a stopping criterion the number of particles grows exponentially. For a growth according to a Heitler model with a production of  $M_{\text{ch}}$  particles after each length  $d_I$ , the number of charged particles at depth  $X$  would be

$$N = M_{\text{ch}}^{X/d_I} , \quad X < n_c d_I . \quad (11)$$

The latter agrees with the result (10) if

$$d_I = \lambda_I \frac{\ln M_{\text{ch}}}{M_{\text{ch}} - 1} . \quad (12)$$

The latter expression is an asymptotic value corresponding to the situation where no stopping criterium is implemented. In the initial stage of the shower the production length  $d_I$  is far from the asymptotic value for the following reason. When the number of particles in the shower is large, the probabilities of the Poisson distribution can be regarded as fractions of the shower. However, when the number of particles in the shower is small, as is the case in the early stage of a shower, the fractions become meaningless: events with such small probabilities will not be realized. In particular for the single initial particle the mean depth at which it interacts is  $\lambda_I$  and not the  $d_I$  as given by (12). Without a stopping criterion the asymptotic value would be reached in a few steps. In reality the stopping mechanism

limits the number of interactions. As a consequence the growth is substantially reduced already after a few steps. This results in values for  $d_I$  larger than the limit value (12), after some more steps to even larger values than  $\lambda_I$ .

What we need for the present analysis is a mean value of  $d_I$ , averaged over the cascade. To obtain this value we consider the limited growth model for several different multiplicities. For this pure mathematical investigation there is no need to distinguish between charged and full multiplicities. We will take a single mathematical multiplicity, conveniently denoted as  $\mu$ . Also for convenience, we describe the situation with respect to a dimensionless depth  $t$  in units of interaction length:  $t = X/\lambda_I$ . The maximum number of interactions (until the charged pions decay) will be denoted as  $k_{\max}$ . Then the expectation value of the number of particles at depth  $t$  is

$$N = \sum_{k=0}^{k_{\max}} \frac{(\mu t)^k}{k!} e^{-t} . \quad (13)$$

The multiplicities we will consider are  $\mu = 2, 3, 5$  and  $10$ . For each  $\mu$  we take the value of  $k_{\max}$  such that  $\mu^{k_{\max}} \approx 1.5 \cdot 10^6$ . That is,  $k_{\max} = 20, 13, 9$  and  $6$  respectively. If the stopping energy is about  $20$  GeV these figures correspond to primary energies of about  $30$  PeV. We mention the latter to give an idea, although the relation with physics is redundant. On the basis of the truncated summation (13) the particle number  $N$  is plotted against  $t$  for  $\mu = 2, 3, 5$  and  $10$ , see the dashed curves in the four separate diagrams of Fig. 2. The first term in (13),  $e^{-t}$ , is the probability for a particle to survive a depth  $t$ . On the basis of this probability also full Monte Carlo simulations are made of the survival lengths of each individual particle in a shower. The number of particles at a certain depth, obtained by binning, are shown as solid curves in Fig. 2.

Although the Monte Carlo simulation is more realistic, it has the disadvantage that every generated shower is a particular realization and not a statistical mean. Every simulation results in a slightly different curve. Therefore there is no sense in a precise comparison between the curves in Fig. 2. It does however show the general agreement between the shower development based on a Monte Carlo simulation and on the Poisson distribution. In both cases the depth of maximum shower size is about  $k_{\max}$ . To obtain a more precise analytical estimate of the depth of maximum shower size we will make use of the fact that the number of particles according to the truncated series (13) follows a similar curve as the number of particles corresponding to the last term of the series (13). A plot of the first differs from a plot of the latter just by a small shift  $\delta$  towards a smaller depth and by a larger amplitude. Denoting the amplitude ratio as  $A$ , we have

$$\sum_{k=0}^{k_{\max}} \frac{(\mu t)^k}{\Gamma(k+1)} \approx \frac{A (\mu t)^{k_{\max}-\delta}}{\Gamma(k_{\max}+1-\delta)} , \quad (14)$$

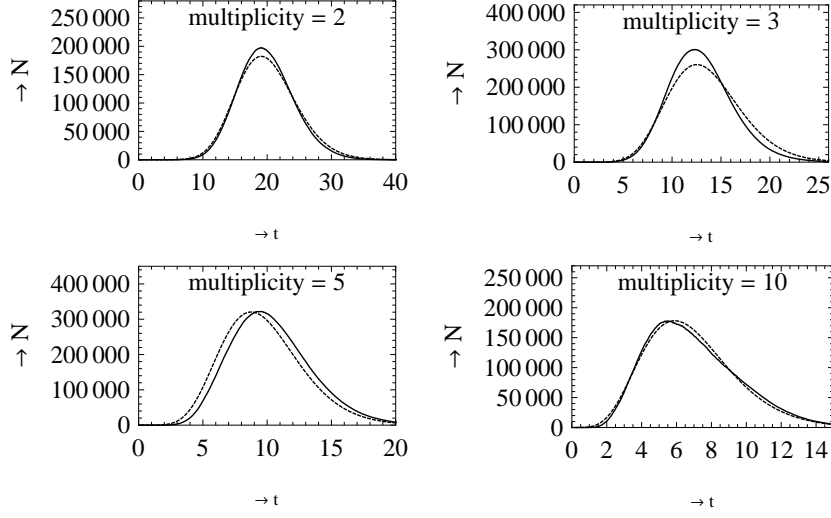


Figure 2: The number of particles against depth in units of interaction length for the following pairs of multiplicity and  $k_{\max}$ : (2,20) (upper left), (3,13) (upper right), (5,9) (lower left) and (10,6) (lower right), on the basis of the truncated series (13) (dashed) and on the basis of a full simulation where each individual particle is tracked (solid).

where  $\Gamma$  is the Gamma function. Substitution in the identity

$$\sum_{k=0}^{k_{\max}+1} \frac{(\mu t)^k}{\Gamma(k+1)} = \frac{(\mu t)^{k_{\max}+1}}{\Gamma(k_{\max}+2)} + \sum_{k=0}^{k_{\max}} \frac{(\mu t)^k}{\Gamma(k+1)} \quad (15)$$

leads to the equation

$$\frac{A(\mu t)^{k_{\max}+1-\delta}}{\Gamma(k_{\max}+2-\delta)} \approx \frac{(\mu t)^{k_{\max}+1}}{\Gamma(k_{\max}+2)} + \frac{A(\mu t)^{k_{\max}-\delta}}{\Gamma(k_{\max}+1-\delta)} . \quad (16)$$

Evaluating at  $t = k_{\max} + 1 - \delta$ , we obtain

$$A \approx \frac{\mu^{1+\delta}}{\mu-1} \cdot \frac{\Gamma(k_{\max}+2-\delta)}{\Gamma(k_{\max}+2)} \cdot (k_{\max}+1-\delta)^\delta . \quad (17)$$

A series expansion for  $A$  approximately yields

$$A \approx \frac{\mu^{1+\delta}}{\mu-1} \cdot \left( 1 - \frac{\delta(\delta+1)}{2k_{\max}} \right) . \quad (18)$$

By numerical inspection it is found that good fits are obtained for

$$\delta \approx \frac{1}{\mu-1} . \quad (19)$$

For the four pairs of values  $(\mu, k_{\max}) = (2, 20)$ ,  $(3, 13)$ ,  $(5, 9)$  and  $(10, 6)$  the number of particles is plotted according to the approximation

$$N \approx \frac{A(\mu t)^{k_{\max}-\delta}}{\Gamma(k_{\max} + 1 - \delta)} e^{-t}, \quad (20)$$

with  $\delta$  as given by (19) and  $A$  as given by (18), see solid curves in Fig. 3. For comparison the number of particles is plotted according to the truncated summation (13) as well, see the dashed curves in Fig. 3.

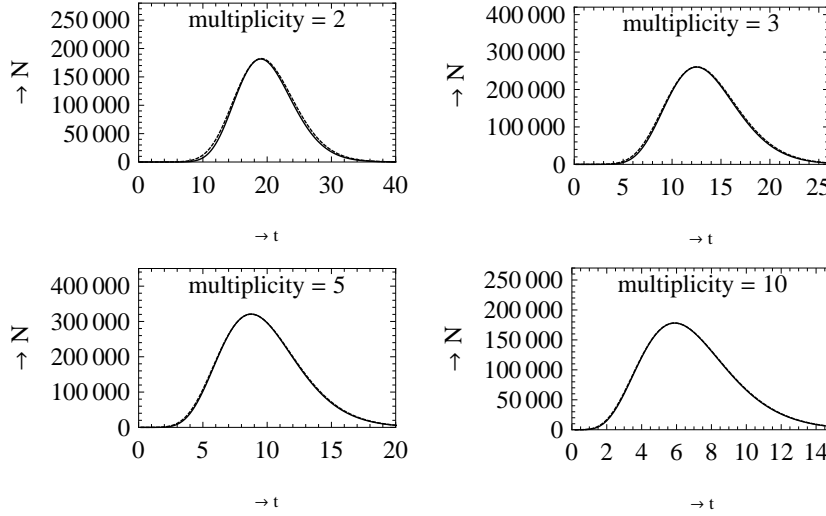


Figure 3: The number of particles against depth in units of interaction length for the following pairs of multiplicity and  $k_{\max}$ :  $(2, 20)$  (upper left),  $(3, 13)$  (upper right),  $(5, 9)$  (lower left) and  $(10, 6)$  (lower right), on the basis of the truncated series (13) (dashed) and on the basis of the approximation (20) (solid).

The two curves in each diagram of Fig. 3 are practically identical; they can hardly be distinguished. The agreement even increases with multiplicity. Therefore approximation (20) can be used for the analytic determination of the depth of maximum shower size. From the approximation (20) it follows that  $N(t)$  reaches its maximum when  $t = k_{\max} - \delta$ . If we return to physics for a moment, in hadronic interactions the multiplicity is of order 10 and larger. The corresponding values for  $\delta$  is smaller than 0.1 and can in practice be neglected:  $t_{\max} \approx k_{\max}$ .

The conclusion of the whole analysis is that the most probable interaction length is  $X_{\max}/k_{\max} = \lambda_I$ . For this reason we take  $d_I = \lambda_I$  as the characteristic length over which the number of particles is increased by a factor  $\mu$ . For clarity,  $d_I < \lambda_I$  in the initial stage of the shower when the shower



number is exponentially growing and  $d_I > \lambda_I$  when the number of particles in the shower approaches its maximum. As a cascade average  $d_I = \lambda_I$ . We therefore will take  $d_I = \lambda_I$  in the present model. In this respect we deviate from Matthews and Hörandel who take  $d_I = \lambda_I \ln 2$  [2, 3].

## 4 The hadronic cascade for a primary proton

Now we consider a hadronic cascade where the hadronic particles interact after having traversed a layer of atmosphere. As argued in the previous section the thickness of each layer will be taken equal to the actual interaction length  $\lambda_I$  as given by (7) or (8). After each interaction  $M$  pions are produced as given by (6). In accordance with the Heitler model for electromagnetic showers, the energy is assumed to be equally divided over the particles produced. After each interaction the new energy of the charged hadrons then follows from a successive application of the equation

$$E_{j+1} = \frac{E_j}{M(E_j)} . \quad (21)$$

Starting with a primary proton with energy  $E_0$  the energy of the particles after the first interaction is

$$E_1 = \frac{E_0}{0.15 \cdot E_0^{0.18}} \approx 6.7 \cdot E_0^{0.82} . \quad (22)$$

After the second interaction this is

$$E_2 = \frac{E_1}{0.15 \cdot E_1^{0.18}} \approx 6.7 \cdot E_1^{0.82} \approx 6.7^{1.82} \cdot E_0^{0.82^2} . \quad (23)$$

Repeating the iteration we find for the energy per particle after  $n$  interactions

$$E_n = 6.7^{\alpha_n} \cdot E_0^{\beta_n} , \quad (24)$$

where

$$\alpha_n = \frac{1 - 0.82^n}{1 - 0.82} , \quad \beta_n = 0.82^n . \quad (25)$$

For the interaction lengths we obtain for the primary proton,  $n = 0$ ,

$$\lambda_0 = \lambda_{p\text{-air}}(E_0) = 145 - 2.3 \ln(E_0) \quad (26)$$

and for the produced pions,  $n \geq 1$ ,

$$\lambda_n = \lambda_{\pi\text{-air}}(E_n) = 200 - 3.3 \ln(E_n) . \quad (27)$$

With the substitution of (24) this is

$$\lambda_n = 200 - 6.3\alpha_n - 3.3\beta_n \ln(E_0) , \quad n \geq 1 . \quad (28)$$

The atmospheric depth of the  $n_c$ -th interaction is given by

$$X(n_c) = \sum_{n=0}^{n_c-1} \lambda_n, \quad n_c \geq 1. \quad (29)$$

Substitution of (26) and (28) leads to

$$X(n_c) = 200n_c - 55 - 6.3 \sum_{n=1}^{n_c-1} \alpha_n - \left( 2.3 + 3.3 \sum_{n=1}^{n_c-1} \beta_n \right) \ln(E_0). \quad (30)$$

With the approximate relation (3) between height and atmospheric depth, we obtain for the difference in height between the  $n_c$ -th and  $(n_c + 1)$ -th interaction:

$$\Delta h[\text{km}] = 8 \ln \left( \frac{X(n_c + 1)}{X(n_c)} \right). \quad (31)$$

For the decay length of the charged pions after the  $n_c$ -th interaction we find

$$c\tau\gamma[\text{km}] \approx 7.8 \cdot 10^{-3} \frac{E_{n_c}}{m_{\pi\pm}} \approx 5.6 \cdot 10^{-11} \cdot 6.7^{\alpha_{n_c}} \cdot E_0^{\beta_{n_c}}, \quad (32)$$

where we have taken  $140 \text{ MeV}/c^2$  for the mass of the charged pions [6]. We will follow Matthews with the reasonable assumption that the pions will decay when the decay length is half the layer thickness:  $\gamma c\tau \approx \frac{1}{2} \Delta h$  [2]. That is

$$5.6 \cdot 10^{-11} \cdot 6.7^{\alpha_{n_c}} \cdot E_0^{\beta_{n_c}} = 4 \ln \left( \frac{X(n_c + 1)}{X(n_c)} \right), \quad (33)$$

In this equation we substitute integer values for  $n_c$  and solve numerically for the primary energy  $E_0$ . Results of interest are shown in table 1, 2 and 3. In table 1 the height  $h$  is calculated with Eq. (3). In table 2 and 3 the interaction lengths respectively multiplicities are given for all interactions up to the final one after which decay occurs.

$n_c$	$E_0$ [eV]	$X(n_c)$	$X(n_c + 1)$	$h(n_c)$ [km]	$\Delta h$ [km]	$\xi_c^\pi$ [eV]
1	$1.5 \cdot 10^{12}$	81	198	20.4	7.2	$6.4 \cdot 10^{10}$
2	$2.9 \cdot 10^{13}$	184	303	13.8	4.0	$3.6 \cdot 10^{10}$
3	$1.4 \cdot 10^{15}$	275	396	10.6	2.9	$2.6 \cdot 10^{10}$
4	$1.9 \cdot 10^{17}$	352	473	8.6	2.4	$2.1 \cdot 10^{10}$
5	$8.2 \cdot 10^{19}$	409	531	7.4	2.1	$1.9 \cdot 10^{10}$

Table 1: Characteristics of hadronic cascades for a primary proton.

$n_c$	$E_0$ [eV]	$\lambda_0$	$\lambda_1$	$\lambda_2$	$\lambda_3$	$\lambda_4$	$\bar{\lambda}$
1	$1.5 \cdot 10^{12}$	81	–	–	–	–	81
2	$2.9 \cdot 10^{13}$	74	110	–	–	–	92
3	$1.4 \cdot 10^{15}$	65	99	111	–	–	92
4	$1.9 \cdot 10^{17}$	53	86	100	112	–	88
5	$8.2 \cdot 10^{19}$	40	70	87	101	112	82

Table 2: Subsequent interaction lengths in hadronic cascades for a primary proton. The  $\lambda_n$  and the cascade average  $\bar{\lambda}$  are in  $\text{g cm}^{-2}$ .

$n_c$	$E_0$ [eV]	$M_0$	$M_1$	$M_2$	$M_3$	$M_4$	$\bar{M}$
1	$1.5 \cdot 10^{12}$	23	–	–	–	–	23
2	$2.9 \cdot 10^{13}$	40	20	–	–	–	28
3	$1.4 \cdot 10^{15}$	80	36	19	–	–	38
4	$1.9 \cdot 10^{17}$	193	75	34	18	–	55
5	$8.2 \cdot 10^{19}$	576	183	72	33	18	85

Table 3: Subsequent multiplicities and their geometric mean in hadronic cascades for a primary proton.

The number of muons is given by

$$N_\mu = \left(\frac{2}{3}\right)^{n_c} \cdot \prod_{n=0}^{n_c-1} M_n . \quad (34)$$

For a primary proton with energy  $1.4 \cdot 10^{15}$  eV, as an example, there will be produced about  $1.6 \cdot 10^4$  muons. The energy of the final pions is about  $2.6 \cdot 10^{10}$  eV, see last entry of table 1. For the quantity

$$\beta = \frac{\ln N_\mu}{\ln (E_0/\xi_c^\pi)} \quad (35)$$

we then obtain the value 0.89. For other primary energies the value of  $\beta$  is found to increase slightly from 0.88 through 0.92 for a primary energy increasing from  $10^{12}$  eV through  $10^{20}$  eV. Since we work with larger multiplicities, these values are slightly larger than the one obtained by Matthews [2].

From the last column in table 3 we find the following approximate relation between the effective multiplicity (the geometric mean multiplicity) and the primary energy:  $\ln \bar{M} \approx 1.05 + 0.074 \ln E_0$ . The effective charged multiplicity then is given by  $\ln \bar{M}_{\text{ch}} \approx 0.65 + 0.074 \ln E_0$ . Substituting the latter in the Matthews' expression [2]

$$\beta = 1 - \frac{\kappa}{3 \ln M_{\text{ch}}} , \quad (36)$$

where  $\kappa$  is the inelasticity, we obtain a refinement for the energy dependence:

$$\beta = 1 - \frac{\kappa}{1.9 + 0.22 \ln E_0} . \quad (37)$$

## 5 Hybrid Heitler scheme

The Heitler line of reasoning can also be applied to electromagnetic shower profiles other than the Heitler profile (1). Let  $N(X; E)$  be an electromagnetic shower profile which for a primary energy  $E$  has its maximum  $N_{\text{max}}(E)$  at depth  $X_{\text{max}}(E)$ . For twice the primary energy the particle will split into two particles with energy  $E$  after one splitting length  $d = \lambda_r \ln 2$ . The corresponding shower profile can be regarded as twice the shower profile for  $E$  shifted with  $d$  towards a larger depth. As a consequence  $N_{\text{max}}(2E) = 2N_{\text{max}}(E)$  and  $X_{\text{max}}(2E) = X_{\text{max}}(E) + d$ . The elongation rate therefore is

$$\frac{dX_{\text{max}}}{d \ln E} = \lambda_r . \quad (38)$$

This scheme will be applied to the present hadronic cascades. Each time when neutral pions decay into photons an electromagnetic subshower is initiated and the corresponding longitudinal profile is substituted. It is similar to what is done in the hybrid Monte Carlo model CONEX [16]. For the electromagnetic shower profile we take the Greisen function [17]:

$$N_e(X) = \frac{0.31}{\sqrt{y_c}} \cdot e^{\frac{X}{\lambda_r}(1-1.5 \ln s)} , \quad (39)$$

where  $y_c = \ln(E_0/\xi_c^e)$  and where

$$s = \frac{3X}{X + 2X_{\max}} \quad (40)$$

is the age parameter. For showers initiated by a photon a good prediction for the depth of maximum is given by

$$X_{\max,\gamma} [\text{g cm}^{-2}] = n_c \cdot d = y_c \cdot \lambda_r \approx 37 \ln E_0 - 675 . \quad (41)$$

For energies larger than 1 EeV, the depth of maximum for photon showers is larger than predicted by (41) because of the Landau-Pomeranchuk-Migdal (LPM) effect [19, 20, 21]. See for instance the corresponding curve in Fig. 13 of [18]. By means of a hybrid Monte Carlo model the consequences of the LPM effect for hadronic air showers are found negligible for primary energies below  $3 \cdot 10^{20}$  eV [8]. For such extremely high primary energies the large multiplicity causes the energy of the decay photons after the first interaction to be below 1 EeV, outside the LPM regime. We will therefore conveniently take (41) for the depth of maximum shower size of electromagnetic (sub)showers. The total electromagnetic shower profile is obtained by adding the profiles of the electromagnetic subshowers. An illustration is given in Fig. 4.

The maximum number of electrons and positrons of the total electromagnetic shower is found by numerical inspection. This semi-analytical approach is utilized to be able to consider all the generations of subshowers. The number of muons is found by means of Eq. (34). In Fig. 5 we have plotted the maximum size of the total electromagnetic shower and the number of muons as a function of initial energy.

A linear fit, see the dashed lines in Fig. 5, for the maximum number of electrons ( $\pm$ ) and number of muons yields

$$N_e \approx 0.57 \cdot (E_0[\text{GeV}])^{1.019} \quad (42)$$

and

$$N_\mu \approx 0.015 \cdot (E_0[\text{GeV}])^{0.975} \quad (43)$$

respectively. The values of  $N_e + 25N_\mu$  for different values of the primary proton energy  $E_0$  are close to the ones obtained with Monte Carlo models, e.g. Fig. 3 of [22].

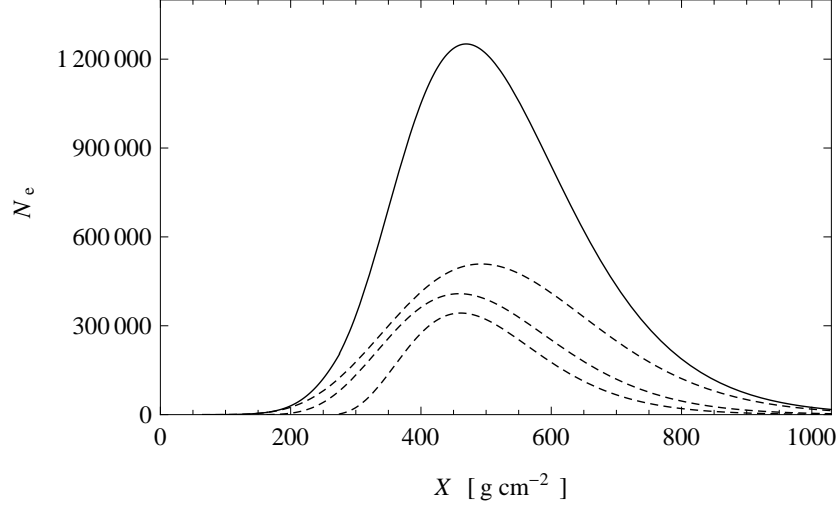


Figure 4: Total electromagnetic shower profile (solid) as it results from the addition of the profiles of the electromagnetic subshowers (dashed) for a 1.4 PeV proton primary.

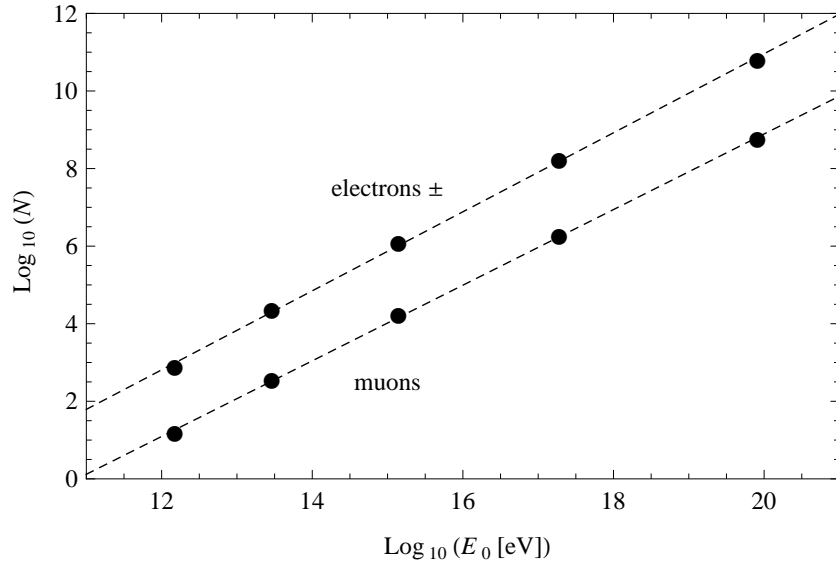


Figure 5: The maximum number of electrons ( $\pm$ ) and muons as a function of the energy of the primary proton (dots) and the linear fits (dashed).

The depth of the maximum shower size of the total electromagnetic shower is also determined by numerical inspection. In Fig. 6 the depth of maximum shower size is plotted as a function of the energy of the primary proton.

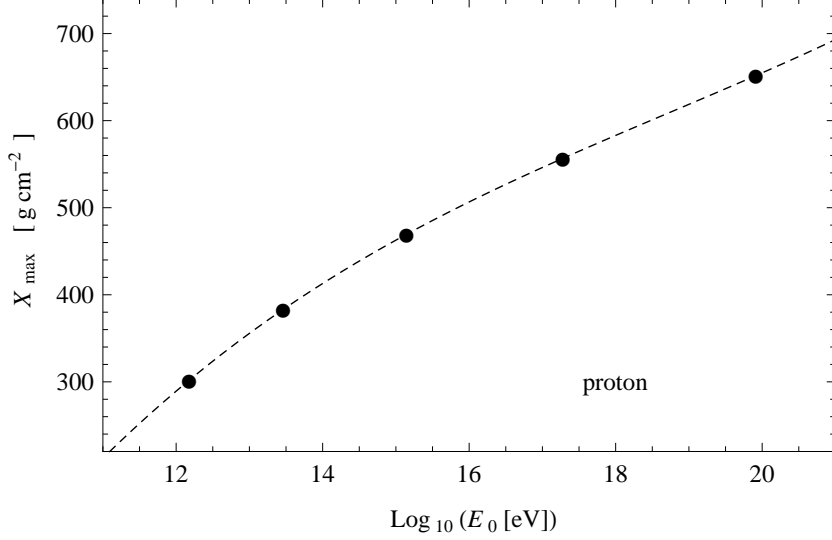


Figure 6: The depth of maximum shower size as a function of energy of a proton primary for the situation without elasticity (dots) and a cubic fit (dashed).

A cubic fit, see the dashed line in Fig. 6, yields

$$X_{\text{max,p}} \approx -1796 + 136.5 \ln E_0 - 2.810(\ln E_0)^2 + 0.0217(\ln E_0)^3 . \quad (44)$$

The latter is the result for a primary proton as indicated by the subscript  $p$ . The cubic fit is plotted to show that the results of the present model neatly follow it. However, the model itself is a simplification of reality and therefore not accurate. Given all the caveats to obtain the present model, a linear fit may be more appropriate:

$$X_{\text{max,p}} \approx -223 + 19.4 \ln E_0 . \quad (45)$$

The latter will be used for a comparison with Monte Carlo results in the final section. An analytical estimate can be obtained by considering solely the first generation of  $\gamma$ 's [2, 3]. Then, with the present model parameters,

$$X_{\text{max,p}} \approx \lambda_{\text{p-air}} + X_{\text{max},\gamma}(E_0/(2M)) \approx -485 + 28 \ln E_0 . \quad (46)$$

Clearly, the elongation rate in the latter expression is substantially larger than in Eq. (45). It is of application to small energies where there is a single generation of  $\gamma$ 's. For larger energies the elongation rate is overestimated by Eq. (46).

## 6 Iron primary

The hadronic cascade for an iron primary differs from the one for a proton primary by a smaller depth of first interaction and by a larger multiplicity in the first interaction. The iron-air cross section is about 2000 mb, see Fig. 54 of [23]. The corresponding interaction length is  $\lambda_{\text{Fe-air}} \approx 12 \text{ g cm}^{-2}$ . The relatively small energy dependence of the iron-air cross section will only lead to a negligible difference of a few  $\text{g cm}^{-2}$ . According to the superposition model [17] the multiplicity of a composite nucleus with atomic mass  $A$  is equal to  $A$  times the multiplicity of a proton with a  $A$  times smaller energy:

$$M_{ch} = 0.1A \cdot \left( \frac{E_0}{A} \right)^{0.18}. \quad (47)$$

For iron-air,  $A = 56$ , this is  $M_{ch} = 2.7 \cdot E_0^{0.18}$ . Since not all nucleons will participate in the same rate as a single proton, the latter should be multiplied by a factor smaller than unity. If this factor is (almost) independent on energy, the superposition model predicts a constant rate between the iron-air and proton-air multiplicity. This is indeed what is seen from QCD based models and from a color glass condensate approach, see Fig. 5 of [7] and Fig. 7 of [24]. On the basis of Fig. 5 of [7] we take in our model the iron-air multiplicity as

$$M_{ch} = 0.3E_0^{0.18}, \quad M = 0.45E_0^{0.18}. \quad (48)$$

In the absence of elasticity the iron-air multiplicity is only present in the first interaction. Except for these two adaptations the analysis is identical to the one for a primary proton. Starting with a primary iron with energy  $E_0$  the energy of the particles after the first interaction is

$$E_1 = \frac{E_0}{0.45 \cdot E_0^{0.18}} \approx 2.2 \cdot E_0^{0.82}. \quad (49)$$

Without elasticity the subsequent interactions are governed by the pion multiplicity:

$$E_2 = \frac{E_1}{0.15 \cdot E_1^{0.18}} \approx 6.7 \cdot E_1^{0.82}. \quad (50)$$

Repeating the iteration we find for the energy per particle after  $n$  interactions

$$E_n = 6.7^{\alpha_{n-1}} \cdot E_1^{\beta_{n-1}}, \quad (51)$$

where  $\alpha_n$  and  $\beta_n$  are as defined in section 3. Substitution of (49) gives

$$E_n = 6.7^{\alpha_{n-1}} \cdot 2.2^{\beta_{n-1}} \cdot E_0^{\beta_n}, \quad (52)$$

For the interaction lengths we have for the primary iron,  $n = 0$ ,

$$\lambda_0 = \lambda_{\text{Fe-air}}(E_0) = 12. \quad (53)$$



The interaction lengths for the produced pions,  $n \geq 1$ , are as given before.

$$\lambda_n = \lambda_{\pi\text{-air}}(E_n) = 200 - 3.3 \ln(E_n) . \quad (54)$$

With the substitution of (52) this is

$$\lambda_n = 200 - 6.3\alpha_{n-1} - 2.6\beta_{n-1} - 3.3\beta_n \ln(E_0) , \quad n \geq 1 . \quad (55)$$

The atmospheric depth of the  $n_c$ -th interaction,  $n_c \geq 1$ , becomes

$$\begin{aligned} X(n_c) = & 200n_c - 188 - 6.3 \sum_{n=1}^{n_c-1} \alpha_{n-1} \\ & - 2.6 \sum_{n=1}^{n_c-1} \beta_{n-1} - 3.3 \ln(E_0) \sum_{n=1}^{n_c-1} \beta_n . \end{aligned} \quad (56)$$

For the decay length of the charged pions after the  $n_c$ -th interaction we now find

$$c\tau\gamma[\text{km}] \approx 5.6 \cdot 10^{-11} \cdot 6.7^{\alpha_{n_c-1}} \cdot 2.2^{\beta_{n_c-1}} \cdot E_0^{\beta_{n_c}} . \quad (57)$$

So, for the depth of the decay of the pions we obtain the following equation:

$$5.6 \cdot 10^{-11} \cdot 6.7^{\alpha_{n_c-1}} \cdot 2.2^{\beta_{n_c-1}} \cdot E_0^{\beta_{n_c}} = 4 \ln \left( \frac{X(n_c + 1)}{X(n_c)} \right) . \quad (58)$$

As before, we substitute integer values for  $n_c$  and solve numerically for the primary energy  $E_0$ . Results of interest are shown in table 4, 5 and 6, the equivalents of table 1, 2 and 3.

$n_c$	$E_0$ [eV]	$X(n_c)$	$X(n_c + 1)$	$h(n_c)$ [km]	$\Delta h$ [km]	$\xi_c^\pi$ [eV]
1	$1.9 \cdot 10^{13}$	12	127	35.6	18.9	$1.7 \cdot 10^{11}$
2	$1.8 \cdot 10^{14}$	121	239	17.2	5.5	$4.9 \cdot 10^{10}$
3	$7.7 \cdot 10^{15}$	221	341	12.3	3.5	$3.1 \cdot 10^{10}$
4	$9.4 \cdot 10^{17}$	309	430	9.6	2.6	$2.4 \cdot 10^{10}$
5	$3.8 \cdot 10^{20}$	380	502	8.0	2.2	$2.0 \cdot 10^{10}$

Table 4: Characteristics of hadronic cascades for a primary iron.

For the energy entries in table 4 the maximum number of electrons and muons for an iron initiated air shower is calculated in a similar way as for the proton initiated air showers. The resulting curves, see Fig. 7, are practically identical to the ones for a proton primary in Fig. 5. A linear fit, see the

$n_c$	$E_0$ [eV]	$\lambda_0$	$\lambda_1$	$\lambda_2$	$\lambda_3$	$\lambda_4$	$\bar{\lambda}$
1	$1.9 \cdot 10^{13}$	12	–	–	–	–	12
2	$1.8 \cdot 10^{14}$	12	109	–	–	–	60
3	$7.7 \cdot 10^{15}$	12	98	110	–	–	74
4	$9.4 \cdot 10^{17}$	12	85	100	111	–	77
5	$3.8 \cdot 10^{20}$	12	69	86	101	112	76

Table 5: Subsequent interaction lengths in hadronic cascades for a primary iron. The  $\lambda_n$  and the cascade average  $\bar{\lambda}$  are in  $\text{g cm}^{-2}$ .

$n_c$	$E_0$ [eV]	$M_0$	$M_1$	$M_2$	$M_3$	$M_4$	$\bar{M}$
1	$1.9 \cdot 10^{13}$	110	–	–	–	–	110
2	$1.8 \cdot 10^{14}$	165	22	–	–	–	60
3	$7.7 \cdot 10^{15}$	325	38	20	–	–	63
4	$9.4 \cdot 10^{17}$	773	78	36	19	–	80
5	$3.8 \cdot 10^{20}$	2274	189	73	34	18	114

Table 6: Subsequent multiplicities and their geometric mean in hadronic cascades for a primary proton.

dashed lines in Fig. 7, for the maximum number of electrons ( $\pm$ ) and number of muons yields

$$N_e \approx 0.59 \cdot (E_0[\text{GeV}])^{1.010} \quad (59)$$

and

$$N_\mu \approx 0.0055 \cdot (E_0[\text{GeV}])^{1.016} \quad (60)$$

respectively. As for proton primaries, the values of  $N_e + 25N_\mu$  for different values of primary iron energy  $E_0$  are close to the ones obtained with Monte Carlo models, see Fig. 3 of [22].

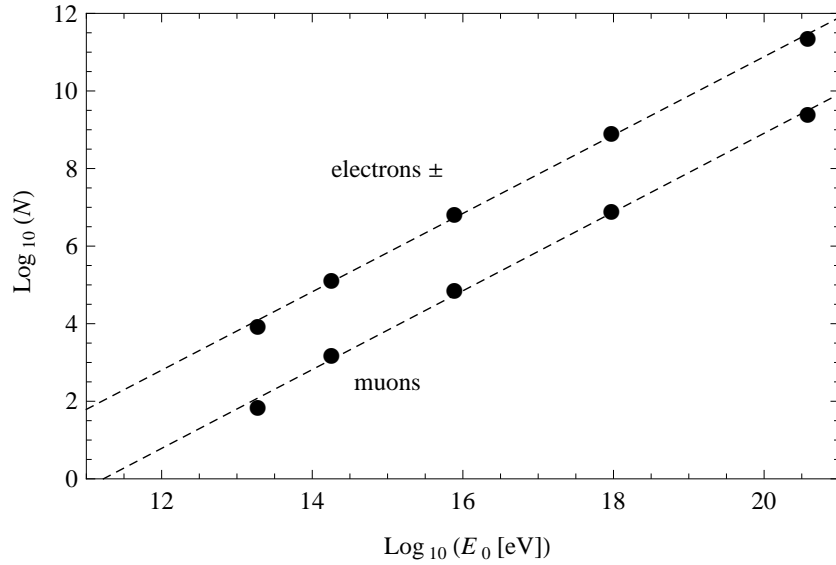


Figure 7: The maximum number of electrons ( $\pm$ ) and muons as a function of the energy of the primary iron (dots) and the linear fits (dashed).

Also the depth of maximum shower size for an iron primary is calculated in a similar way as for a proton primary. The result is shown in Fig. 8.

Both the smaller interaction length and the larger multiplicity have reduced the depth of maximum shower size with respect to a proton initiated shower. A cubic fit, see the dashed line in Fig. 8, yields

$$X_{\text{max,Fe}} \approx -2116 + 143.0 \ln E_0 - 2.721(\ln E_0)^2 + 0.0194(\ln E_0)^3, \quad (61)$$

where the subscript Fe identifies the primary particle. A linear fit yields

$$X_{\text{max,Fe}} \approx -345 + 20.6 \ln E_0. \quad (62)$$

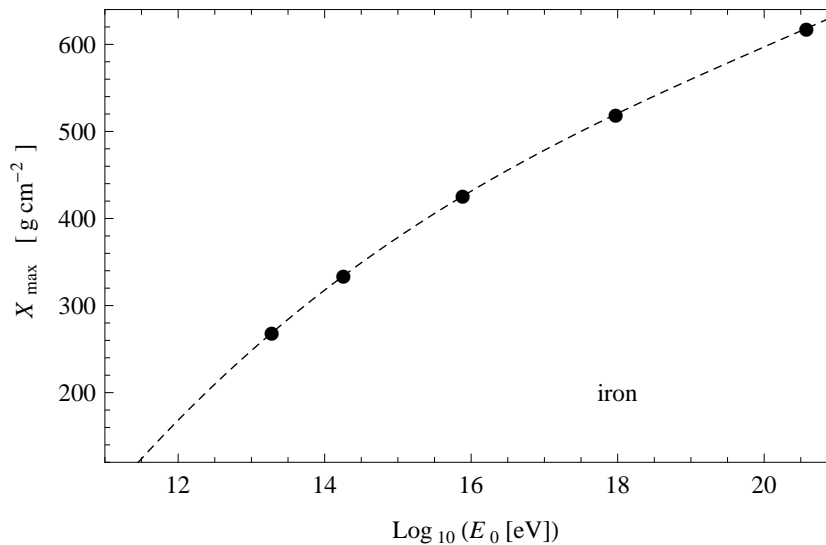


Figure 8: The depth of maximum shower size as a function of energy of an iron primary for the situation without elasticity.

As for the proton a completely analytical estimate can be obtained by considering solely the first generation of  $\gamma$ 's:

$$X_{\text{max,Fe}} \approx \lambda_{\text{Fe-air}} + X_{\text{max},\gamma}(E_0/(2M)) \approx -659 + 28 \ln E_0 . \quad (63)$$

Also here the elongation rate in the analytical expression is substantially larger than in Eq. (62).

## 7 Conclusions and discussion

Hadronic cascades in cosmic air showers are analyzed by means of a Heitler-Matthews model extended to all generations of pions. For all the predictions a multiplicity and interaction length is applied parameterized for energy. It is argued that the thickness of the interaction layers should be taken equal to the interaction length and not a fraction  $\ln 2$  of it. Although this increases the prediction for the depth of maximum shower size with a few tens of  $\text{g cm}^{-2}$ , the value for  $X_{\text{max}}$  still is too small. It is also shown that an analysis based on the first generation of  $\gamma$  showers leads to an overestimation of the elongation rate. This implies that the agreement with the elongation rate as predicted by Monte Carlo models may be accidental. It also implies that the neglect of the second and further generations of  $\gamma$ 's can not explain the discrepancy between the depth of maximum shower size as predicted by the Heitler-Matthews model and as predicted by Monte Carlo models. An alternative explanation is proposed below.

For a proton and iron primary the depth of maximum shower size as predicted by Monte Carlo models, see for instance the right panel of Fig. 10 of [9], Fig. 13 of [18] or Fig. 9 of [25], is about

$$X_{\max,p} \approx -275 + 24 \ln E_0 \quad (64)$$

and

$$X_{\max,Fe} \approx -585 + 29 \ln E_0 \approx 1.5 \cdot (-345 + 20.6 \ln E_0) \quad (65)$$

respectively. These values are about 25% respectively 50% larger than as predicted by the present model:

$$-275 + 24 \ln E_0 \approx 1.25 \cdot (-223 + 19.4 \ln E_0) \quad (66)$$

respectively

$$-585 + 29 \ln E_0 \approx 1.5 \cdot (-345 + 20.6 \ln E_0) . \quad (67)$$

In other words, for a primary proton the discrepancy is about  $\frac{1}{4} X_{\max,p}$ .

As a consequence of the Heitler-Matthews model the energy of the interaction is equally divided over the secondary particles. In reality the distribution of energy is highly inhomogeneous. This is observed in proton-proton collisions, see Fig. 48 of [26]. For proton-air collisions it is predicted by Monte Carlo models, see Fig. 6 of [18]. Many secondary's obtain a small part of the energy while a few particles obtain a larger part. The elasticity effect, where a substantial part of the energy is taken by the leading particle, can be regarded as the most profound manifestation of the inhomogeneous energy distribution. Both the elasticity and the inhomogeneous energy distribution over the non-leading secondary's increase the depth of maximum shower size. In our opinion the equal division of energy is therefore responsible for the discrepancy with respect to shower simulators which have the inhomogeneous energy distribution incorporated. To give some foundation to the idea we consider the following relation [27]:

$$\frac{\Delta X_{\max}}{X_{\max}} \approx -\frac{1}{2} \frac{\Delta M}{M} - \frac{1}{10} \frac{\Delta \kappa}{\kappa} . \quad (68)$$

In this relation  $\Delta X_{\max}$  is the shift of the depth of maximum shower size,  $M$  is the multiplicity and  $\kappa$  is the inelasticity. For protons and pions the inelasticity is roughly about  $\frac{2}{3}$ , see figure 6 of [8]. Starting from the inelastic situation,  $\kappa = 1$ , the change in elasticity is  $\Delta \kappa = -\frac{1}{3}$ . According to the second part in the right hand side of Eq. (68) this corresponds to a shift

$$\Delta X_{\max} \approx \frac{1}{30} \cdot X_{\max} . \quad (69)$$

That is, about 15% of the discrepancy can be explained by elasticity.

Also the inhomogeneous energy distribution over the non-leading secondary's increase the depth of maximum shower size. Among the secondary charged pions there will be a few with relatively large energy who penetrate deeper into the atmosphere thereby contributing to the depth of maximum shower size in a similar way as elasticity does. At the same time there will be many secondary charged pions with energies so low that they will decay before they reach final generation of the cascade. In effect this reduces the cascade mean multiplicity. From the first part of the right hand side of Eq. (68) it follows that a substantial contribution to the shift  $\Delta X$  can be expected. Since the effective reduction of multiplicity will be larger for large multiplicities and thus for large energies, the relative shift will be larger for large energies. As a consequence the inhomogeneous energy distribution over the non-leading secondary's does increase the depth of maximum shower size as well as the elongation rate. Since the multiplicity for iron is larger than for proton primaries, the larger discrepancy for iron primaries supports the idea that the discrepancy is related to the effective multiplicity and thus to the inhomogeneous energy distribution.

Of course, there also is the possibility for other contributions to the discrepancy. For instance, a part of the discrepancy might be an artefact of the discreteness of the hadronic cascade in the present model. We therefore can not say whether the inhomogeneous energy distribution over the non-leading secondary's explains all of the remaining 85% of the discrepancy. It seems however reasonable to expect that the inhomogeneous energy distribution is responsible for a large part of the difference between the depth of maximum shower size as predicted by Monte Carlo models and as predicted by the present model.

## Acknowledgements

I wish to thank Dr. J.J.M. Steijger for his detailed and useful comments on an earlier draft of this paper and prof. J.W. van Holten and Prof. B. van Eijk for their encouragement. I also wish to thank Nikhef for its hospitality. The work is supported by a grant from NWO (Netherlands Organisation for Scientific Research).

## References

- [1] W. Heitler, The Quantum Theory of Radiation, third ed., Oxford University Press, London, p. 386 (1954).
- [2] J. Matthews, Astropart. Phys. **22**, 387 (2005).
- [3] J. R. Hörandel, Mod. Phys. Lett. A, **22**, 1533 (2007).
- [4] R. Ulrich, R. Engel and M. Unger, Phys. Rev. D **83**, 054026 (2011).
- [5] R. engel, D. Heck and T. Pierog, Annu. Rev. Nucl. Part. Sci. **61**, 467 (2011).
- [6] Particle Data Group, Review of particle Physics, J. Phys. G **37**, 31 (2010).
- [7] S. Roesler, R. Engel and J. Ranft, SLAC-PUB-11093, 27th ICRC, Hamburg (2001).
- [8] J. Alvarez-Muñiz et al., Phys. Rev. D **66**, 033011 (2002).
- [9] J. Knapp et al., Astropart. Phys. **19**, 77 (2003).
- [10] R. Ulrich et al., New J. Phys. **11**, 065018 (2009).
- [11] P. Abreu et al, arXiv:1208.1520.v2 (2012).
- [12] M. Aglietta et al., EAS-TOP Collaboration, Phys. Rev. D **79**, 032004 (2009).
- [13] G. Aielli et al, ARGO Collaboration, Phys. Rev. D **80**, 092004 (2009).
- [14] T. Stanev, High Energy Cosmic Rays, 2nd ed., Springer-Verlag Berlin Heidelberg New York, 213 (2003).
- [15] J.M.C. Montanus, Astropart. Phys. **35**, 609 (2012).
- [16] T. Bergmann et al., Astropart. Phys. **26**, 420 (2007).
- [17] T. Gaisser, Cosmic Rays and Particle Physics, Cambridge University Press, Cambridge, p. 224 (1990).
- [18] H. Rebel and O. Sima, Rom. Journ. Phys. **57**, 472, (2012).
- [19] L. D. Landau and I. J. Pomeranchuk, Dokl. Akad. Nauk SSSR **92**, 535, (1953).

- [20] L. D. Landau and I. J. Pomeranchuk, Dokl. Akad. Nauk SSSR **92**, 735, (1953).
- [21] A. B. Migdal, Phys. Rev. **103**, 1811, (1956).
- [22] M.A.K. Glasmacher, Astropart. Phys. **12**, 1 (1999).
- [23] J. Knapp, D. Heck and G. Schatz, Forschungszentrum Karlsruhe Report **FZKA 5828**, (1996).
- [24] HJ. Drescher, arXiv:astro-ph/0612218v1, (2006).
- [25] J. R. Hörandel, J. Phys. G: Nucl. Part. Phys., **29**, 2439 (2003).
- [26] C. Alt et al., Eur. Phys. J. **45**, 343, (2006).
- [27] C. Pajares, D. Sousa and R.A. Vázquez, Astropart. Phys. **12**, 291, (2000).